View metadata, citation and similar papers at core.ac.uk

brought to you by CORE

provided by University of East Anglia digital repository

Hydrothermal synthesis of reduced graphene oxide-$LiNi_{0.5}Mn_{1.5}O_4$ composites as 5 V cathode materials for Li-ion batteries

Mingyue Mo [1], Hongyu Chen [2], Xiaoting Hong [3,*], K.S. Hui [4], Chengcong Ye [2], Ke Lai [2]

[1] *Key Laboratory of Agricultural Products Chemical and Biological Processing Technology of Zhejiang Province，School of Biological and Chemical Engineering, Zhejiang University of Science and Technology, Hangzhou 310023, China*

[2] *School of Chemistry and Environment, South China Normal University, Guangzhou 510006, PR China*

[3] *School of Civil Engineering and Architecture, Zhejiang University of Science and Technology; Key Laboratory of Recycling and Eco-treatment of Waste Biomass of Zhejiang Province, Hangzhou 310023, China*

[4] *Faculty of Science, School of Mathematics, University of East Anglia, Norwich NR4 7TJ, UK*

Corresponding author:

Xiaoting Hong (X.T. Hong), Tel.: +86-0571-85070528.

E-mail address: hanren.xiaoting@gmail.com

Abstract

Composite materials consisting of reduced graphene oxide and $LiNi_{0.5}Mn_{1.5}O_4$ were in-situ prepared by a simple one-step hydrothermal-treating method. The physical property and electrochemical performance of the composite materials were characterized by X-ray diffraction (XRD), Raman spectroscopy, scanning electron microscopy (SEM), X-ray photoelectron spectroscopy (XPS), cyclic voltammetry (CV), charge/discharge testing and electrochemical impedance spectroscopy (EIS). The results demonstrate that the graphene oxide is partially reduced and uniformly in-situ anchored on the surface of $LiNi_{0.5}Mn_{1.5}O_4$. As a result, the specific surface area of the composite material dramatically increases from 0.2488 $m^2 \cdot g^{-1}$ to 8.71 $m^2 \cdot g^{-1}$ and the initial specific discharge capacity improves from 125.8 $mAh \cdot g^{-1}$ to 140.2 $mAh \cdot g^{-1}$, respectively. Furthermore, the capacity retention maintains 95.8 % after 100 cycles and the electrode polarization has significantly been lessened. At rates of 1 C, 2 C and 5 C, the composite material with 5 % reduced graphene oxide can deliver much higher capacities than the pristine $LiNi_{0.5}Mn_{1.5}O_4$. Moreover, AC impedance test results show that the interfacial charge transfer impedance obviously reduced. It's confirmed that the introduction of reduced graphene oxide through hydrothermal treating is effective to enhance the electrochemical performance of the composite material.

Keywords: $LiNi_{0.5}Mn_{1.5}O_4$; reduced graphene oxide; in situ; hydrothermal treating;

1. Introduction

$LiNi_{0.5}Mn_{1.5}O_4$ (LNMO) is considered as one of the most promising lithium-ion battery cathode materials for commercial application with high-power requirements in electric vehicles (EVs) and hybrid electric vehicles (HEVs) because of its low cost, high theoretical specific capacity (146.7 $mAh \cdot g^{-1}$), high operating voltage (4.7 V vs. Li^+/Li) due to the reversible oxidation of Ni^{2+} to Ni^{3+} and Ni^{4+} with lithium de-intercalation [1-2]. However, serious capacity fading of LNMO tends to be encountered attributed to its 4.7 V high operating voltage during the cycling processes especially in the first cycle, mainly caused by the electrolyte decomposition and the Mn dissolution problem attacked by HF [3-5]. Meanwhile, relative low conductivity of LNMO giving rise to poor high-rate performance inevitably limits its practical applications [6].

To solve the problems mentioned above, great efforts have been made to enhance the stability and the electrochemical performance of LNMO through surface modification, cation doping, and synthesis of different nanosized structures [7]. Among various scientific strategies, surface modifications of LNMO have substantially been investigated through coating materials such as ZnO [8], RuO_2 [9], BiOF [10], Li_3PO_4 [11], Al_2O_3 [12] and AlF_3 [13]. Although most of them demonstrated the improvement in the cycle performance of LNMO to different degrees, coating by metal oxides is not much in favor of high rate properties because these inorganic coating layers are not good conductor and extra resistance tends to be inserted into lithium ion batteries according to Liu [7].

Recently, graphene has attracted considerable attention as a promising material for energy application, owing to its high electronic conductivity, large surface area, and excellent structural stability [14]. Graphene has been reported as a conductive additives for $LiNi_{1/3}Co_{1/3}Mn_{1/3}O_2$ [15], $LiFePO_4$ [16], $Li(Li_{0.2}Mn_{0.54}Ni_{0.13}Co_{0.13})O_2$ [17], $LiNi_{0.5}Mn_{1.5}O_4$ [18], and $LiMn_2O_4$ [19] electrodes to enhance the conductivity and protect the electrode surface away from the electrolyte attack in lithium ion batteries. Subsequently, charge transfer resistance can be reduced and the rate capability and cyclability are improved. Reduced graphene oxide (rGO) is usually considered as one kind of chemically derived graphene with high conductivity, prepared via the reduction of graphene oxide (GO) with the recovery of a conjugated structure by removing the oxygen-containing groups [20]. Thus, rGO used in electrode composites for electrochemical systems has achieved greater attention due to the excellent dispersion characteristic of GO and various reduction methods for GO to rGO [21].

In this study, composite materials consisting of reduced graphene oxide and $LiNi_{0.5}Mn_{1.5}O_4$ were in-situ prepared through a simple one-step hydrothermal-treating method. We presented and discussed the structural, morphological properties and electrochemical performance of the composite materials to investigate the effect of the rGO as a coating layer on LNMO as the high voltage cathode material.

2. Experimental

LNMO spinels were prepared by a gelatin-assisted synthetic method referred to our previous work [22]. Composites of LNMO and rGO were in-situ synthesized in

the following procedure. Firstly, 5% graphene oxide (GO, XF NANO) in the weight ratio of 1 g LNMO was put into 100 mL deionized water by ultrasonic dispersing for 30 min. Then the GO dispersion and 1 g LNMO were mixed by mechanical stirring and transferred into an autoclave and maintained at 160 °C for 4 h. The precipitates were centrifuged and washed with the deionized water and ethanol for three times, dried at 80 °C to get the composites of LNMO and rGO, labeled as rGO-LNMO. Black reduced graphene oxide was obtained by the same ultrasonic and hydrothermal treating, labeled as rGO.

The X-ray diffraction (XRD) of the samples was carried out on a Bruker D 8 Advance diffractometer equipped with Cu Kα radiation from 10 ° to 80 ° with a step size of 0.02 °•s^{-1}. The Raman spectra were collected with a Confocal Laser Micro Raman Spectrometer (Labram Aramis, HJY) using an excitation light of 532 nm. The particle morphology was characterized by Zeiss Ultra 55 field-emission scanning electron microscopy (SEM). XPS spectra were obtained on a Thermo-VG Scientific ESCALAB 250 spectrometer.

Electrochemical properties of the pristine and the composite samples were measured using CR-2025 coin cells. The cathode films were prepared by mixing active cathode materials, acetylene black and polyvinylidene fluoride with a weight ratio of 8: 1: 1 in N-methyl-2-pyrrolidone. The slurry was ground for 4 h and coated onto aluminum foil using a blade, then dried at 120 °C under vacuum for 12 h. The dried electrodes, metallic lithium anode, 1 mol•L^{-1} $LiPF_6$ dissolved in ethylene carbonate, dimethyl carbonate and ethylmethyl carbonate solution (EC: DMC: EMC =

1: 1: 1, volume), and Celgard 2400 polypropylene separators were all put into an argon-filled glove box (Mikrouna Universal 2440/750) and finally assembled into CR-2025 coin cells. The cells were galvanostatically cycled between 3.5 and 4.9 V using multi-channel battery testers (Neware CT-3008W) at 25 °C. Cyclic voltammetry (CV) measurements were carried out on an electrochemical workstation (CHI, 660D) at a scanning rate of 0.05 mV s^{-1} over a potential range of 3.2 - 5.0 V. Electrochemical impedance spectra (EIS) tests were conducted in the open circuit voltage state after five cycles at 1 C rate with an AC amplitude of 5 mV in the frequency range from 10^5 Hz to 10^{-1} Hz.

3. Results and discussion

3.1 Materials and discussion

Fig. 1 shows the XRD patterns of LNMO, rGO-LNMO and rGO. All diffraction peaks of LNMO are sharp and well-defined, which indexed to a typical cubic crystal structure (JCPDS No. 80-2162). Minor amounts of secondary phases assigned to rock-salt structures also exist in the powder sample, which are reported to be inevitable components formed in the high-temperature synthetic process of LNMO [23]. It can be observed that the XRD characteristic peaks of LNMO in the rGO-LNMO coincide well with those of the bare sample, suggesting that no spinel structural damage is suffered and no additional impurity phase is imported in the LNMO composite after hydrothermal treatment. However, the diffraction peaks of the reduced graphene oxide at 25.5 ° cannot be found in the XRD pattern of rGO-LNMO,

probably due to the low contents of GO [24].

As shown in Fig. 2 (a), the frequency range between 100 to 700 cm^{-1} in the Raman spectra of rGO-LNMO is corresponded to the Raman spectra of LNMO which is similar to that of ordered LNMO spinel elsewhere [25]. The strong band around 635 cm^{-1} is assigned to the symmetric Mn-O stretching mode of MnO_6 octahedra (A_{1g}), while the two peaks around 494 and 402 cm^{-1} are associated with the Ni^{2+}-O stretching mode in the structure [25]. Meanwhile, the strong band around 161 cm^{-1} is considered as the obvious evidence of the ordered $P4_332$ structure of the spinel. Moreover, there are two Raman bands located at 1323 cm^{-1} and 1597 cm^{-1}, which can be assigned to the D and G bands of rGO, respectively, indicating the successful inclusion of reduced graphene oxide in the composite. For further comparison, the Raman spectra of GO and rGO are displayed in Fig. 2 (b) and (c), respectively. The D band is a breathing mode of κ-point phonons of A_{1g} symmetry, while the G band is usually assigned to the E_{2g} phonon of C sp^2 atoms. A prominent D band is an indication of disorder of the GO in the Raman, originating from defects associated with vacancies, grain boundaries and amorphous carbon species. According to the report of Zhou's group [26], the intensity ratio (I_D/I_G) of D band to G band is related with the extent of π-conjugation and concentration of defects on G band. It can be found that the I_D/I_G ration of the GO is about 1.37 and decreased to 0.95 after hydrothermal treatment, suggesting that a certain extent of GO has been successfully reduced to rGO.

Fig. 3 depicts the SEM images of the morphology of the rGO-LNMO composites.

It can be clearly seen in Fig. 3(a) that the LNMO particles aggregate together and exhibit a regular octahedral shape for the typical spinel structure, wrapped with the rGO sheets on the surface. High magnification SEM in Fig. 3 (b) confirms that the rGO sheets distribute uniformly with a nano-meter size and tightly cling to the surface of the spinel particles.

Fig. 4 shows the energy dispersive X-ray spectroscopy (EDX) mapping of rGO-LNMO under SEM (the mapping area is showed on the top left side). It is obvious that four elements of Ni, Mn, O and C are included in the composite material. Furthermore, the Mn/Ni ratio is 3.1:1, which is in line with the theoretical atomic ratio value of LNMO. Also it can be clearly seen that the mapping of element C, mainly derived from the reduced graphene oxide, has the same distribution as other elements, suggesting that the reduced graphene oxide is uniformly coated onto the LNMO particles. At the same time, the Brunauer-Emmett-Teller (BET) testing results reveal that the specific surface area of rGO-LNMO greatly increases and reaches a value of 8.71 $m^2 \cdot g^{-1}$, while pure LNMO is only 0.2488 $m^2 \cdot g^{-1}$ (Figure S1). Such a composite structure as well as the increased specific surface area might help the electrode material quickly wetted by the electrolyte and facilitate Li^+ transportation in the bulk LNMO. Furthermore, the rGO layer plays a significant role of an effective conductive network to speed up the electron transfer and should contribute to the promotion of the electrochemical properties [1].

XPS analysis of GO, LNMO and rGO-LNMO are carried out in order to gain more insight into the chemical structure characteristics on the surface of the bare and

the composite materials. As shown in Fig. 5(a), the C 1s spectra of GO and LNMO are fitted into three peaks, which can be assigned to carbon atoms in three functional groups: C-C bond (284.6 eV), C-O band (286.8 eV) and C=O band (288.6 eV) [20]. After hydrothermal treatment, both the bonding energies of the C-O band and C=O band for rGO-LNMO powder become weaker compared to GO, further proved that the GO has successfully been reduced to some extent in the composite material. On the other hand, the peak intensities of the C-O band and C=O band for rGO-LNMO powder are observed to be much stronger than the bare spinel powders, indicating the presence of partial rGO with oxygen-containing groups on the surfaces of the powders. As a previous literature reported [24], the rGO can combine with LNMO by an interfacial attraction between the residual oxygen groups of rGO and the dangling OH groups of LNMO through electric field effect and/or hydrogen bonding. Fig. 5 (b) gives the XPS binding energy of Mn 2p and Ni 2p in the bare and the composite materials. No obvious shift in binding energy demonstrates a fixed element valence of Mn and Ni, indicating that the oxidation states of Mn and Ni remain unchanged in the spinel structure before and after the hydrothermal process. Meanwhile, it can be found that the XPS observations agree well with the former XRD and Raman results.

3.2 Electrochemical characterization

The initial charge-discharge voltage profiles of rGO-LNMO and the pristine sample between 3.5 and 4.9 V at 0.1 C are presented in Fig. 6 (a). Both cells show a traditional voltage plateau at 4.7 V attributed to the Ni^{2+}/Ni^{4+} redox reaction and

present a small voltage region of 4.0 V arising from the redox couple of Mn^{3+}/Mn^{4+}. In contrast to the LNMO, the first discharge capacity of the rGO-LNMO sample greatly increases from 125.8 to 140.2 $mAh \cdot g^{-1}$ owing to the improvement in electronic conductivity and the acceleration of lithium ion diffusion by rGO addition [15]. Moreover, the Coulombic efficiency rises up to 92.2 % and the voltage difference between the charge and discharge plateaus of rGO-LNMO becomes smaller, indicating that the polarization and the inner resistance of the batteries have been effectively reduced by wrapping LNMO with the rGO sheets. This result is consistent with the results elsewhere [18], where the Prabakar's group proposed that the graphene layers functioned as a barrier to electrolyte oxidation and higher Coulombic efficiency was obtained.

Cyclic voltammetry (CV) curves of the bare and the composite materials shown in Fig. 6 (b) are in good agreement with the above charge-discharge curves. The high peaks in the high voltage range further strengthens that the total capacity was dominated by the Ni^{2+}/Ni^{4+} redox couples, while the small peaks at 4.0 Vcorrespond to the existence of a minor content of Mn^{3+}. Accordingly, no other reduction peak in the CV curves of the rGO-LNMO was found confirming that wrapping with rGO leads to no extra redox reactions in the testing voltage range, which indicated that the composite material remains an electrochemical stability. Furthermore, compared to the pristine LNMO, the electrochemical activity is obviously improved for the rGO-LNMO composite as the observation of the higher current and larger integrated area of the peak at 4.7 V. Fig. 6 (c) gives the cyclic performance of the pristine and

the rGO-LNMO at 1 C. After 100 cycles, the capacity retention of the pristine and the rGO-LNMO are 95.5 % and 95.8 %, respectively. According to the findings of Monaco's group [1], they evinced that the main cause of the capacity loss over cycling of $LiNi_{0.5}Mn_{1.5}O_4$ is not the dissolution of Mn^{2+} from Mn^{3+} disproportion, instead, an increase in thickness of the passivation surface layer [27, 28]. Therefore, the rGO-LNMO composite electrode shows more stable cycling performance than the pristine LNMO as a cathode in lithium ion batteries.

In order to further confirm the effect of the rGO contents on the electrochemical performance, the rate performance was investigated by four LNMO composite samples with different rGO contents as displayed in Fig. 6 (d). All of the cells are firstly galvanostatically charged at 0.2 C rate, then discharged from 0.1 C rate to 5 C rate, and finally reset to back 0.1 C rate. Compared with the pristine material cathode, discharge capacities of 2.5 % rGO-LNMO, 5 % rGO-LNMO are greatly increased at all the different discharge rates. Meanwhile, 5 % rGO-LNMO deliver higher capacities of 119 $mAh \cdot g^{-1}$, 108.7 $mAh \cdot g^{-1}$ and 93 $mAh \cdot g^{-1}$ at 1 C, 2 C and 5 C rate, which is 90.3 %, 82.5 % and 69.6 % of the discharge capacity at 0.5 C rate, respectively. The improvement in the rate performance of the composite materials completely match and verify our previous testing analysis that the rGO nanosheets can act as a conductive support and favor the lithium ion diffusion and de-intercalation of the cathode materials. However, it can be observed that 10 % rGO-LNMO exhibited lower capacity and worse rate performance due to the dispersion difficulty and agglomerate tendency with excessive amount of rGO [18].

The EIS spectra of the pristine and rGO-LNMO are presented in Fig. 7, with an equivalent circuit in the inset. Both of the two impedance plots are composed of a semicircle in the high frequency range and a straight sloping line in the low frequency range. The semicircle in high frequency is corresponding to the charge transfer impedance (R_{ct}), referred to the charge transfer of lithium ion on the surface of spinel oxide [22], while the straight line in the low frequency is linked with the Warburg impedance (Z_w) caused by the solid-phase diffusion in the electrode materials [29]. It was observed that the diameter of the semicircle in high frequency of the rGO-LNMO sample is decreased significantly, reflecting that the R_{ct} of the rGO-LNMO composite sample has been effectively decreased. Thus, the EIS results further demonstrate the incorporation of rGO by hydrothermal treating is effective to improve the electrochemical performance of the composite materials.

4 Conclusions

We successfully synthesized the composite materials of $LiNi_{0.5}Mn_{1.5}O_4$ and rGO via a simple one-step hydrothermal treating method. The GO was partially reduced and uniformly in-situ anchored on the surface of $LiNi_{0.5}Mn_{1.5}O_4$, while no spinel structural damage is suffered and no additional impurity is imported in the composite material. Compared to the pristine LNMO, the specific surface area of the composite material dramatically increases from 0.2488 $m^2 \cdot g^{-1}$ to 8.71 $m^2 \cdot g^{-1}$, which is favorable for the electrode material to be quickly wetted by the electrolyte. The initial specific discharge capacity improves from 125.8 $mAh \cdot g^{-1}$ to 140.2 $mAh \cdot g^{-1}$. Furthermore, the

capacity retention keeps to 95.8 % after 100 cycles and the electrode polarization has been significantly lessened. Meanwhile, 5 % rGO-LNMO delivers high capacities of 119 $mAh \cdot g^{-1}$, 108.7 $mAh \cdot g^{-1}$ and 93 $mAh \cdot g^{-1}$ at 1 C, 2 C and 5 C rate respectively, and all of them are much higher than those of the pristine LNMO. The AC impedance test results also show that the interfacial charge transfer impedance of the composite material has been effectively decreased. Therefore, the composite materials of LNMO and rGO via the simple one-step hydrothermal treating method could be employed as a very promising candidate cathode material in lithium-ion batteries.

Acknowledgements

Financial support for this work was provided by Zhejiang University of Science and Technology youth talent cultivation plan.

References

[1] S. Monaco, F. De Giorgio, L. Da Col, M. Riche1, C. Arbizzani, M. Mastragostino, Electrochemical performance of $LiNi_{0.5}Mn_{1.5}O_4$ composite electrodes featuring carbons and reduced graphene oxide, J. Power Sources 278 (2015) 733-740.

[2] S. Lee, Y. Cho, H. K. Song, K. T. Lee, J. Cho, Carbon-coated single-crystal $LiMn_2O_4$ nanoparticle clusters as cathode material for high-Energy and high-Power lithium-ion batteries, Angew. Chem. 124 (2012) 8878-8882.

[3] N. P. W. Pieczonka, Z. Liu, P. Lu, K. L. Olson, J. Moote, B. R. Powell, J. H. Kim,

Understanding transition-metal dissolution behavior in $LiNi_{0.5}Mn_{1.5}O_4$ high-voltage spinel for lithium ion batteries, J. Phys. Chem. C 117 (2013) 15947-15957.

[4] J.H. Kim, N. P. W. Pieczonka, Z. Li, Y. Wu, S. Harris, B. R. Powell, Understanding the capacity fading mechanism in $LiNi_{0.5}Mn_{1.5}O_4$/graphite Li-ion batteries, Electrochim. Acta 90 (2013) 556-562.

[5] N. Mahootcheianasl, J.H. Kim, N. P. W. Pieczonka, Z. Liu, Y. Kim, Multilayer electrolyte cell: a new tool for identifying electrochemical performances of high voltage cathode materials, Electrochem. Commun. 32 (2013) 1-4.

[6] J. Liu, A. Manthiram, Understanding the improvement in the electrochemical properties of surface modified 5 V $LiMn_{1.42}Ni_{0.42}Co_{0.16}O_4$ spinel cathodes in lithium-ion cells, Chem. Mater. 21 (2009) 1695-1707.

[7] G.Q. Liu, L. Wen, Y. M. Liu, Review spinel $LiNi_{0.5}Mn_{1.5}O_4$ and its derivatives as cathodes for high-voltage Li-ion batteries, J. Solid State Electronchem. 14 (2010) 2191-2202.

[8] H. Sun, B. Xia, W. Liu, G. Fang, J. Wu, H. Wang, R. Zhang, S. Kaneko, J. Zheng, H. Wang, D. Li, Significant improvement in performances of $LiNi_{0.5}Mn_{1.5}O_4$ through surface modification with high ordered Al-doped ZnO electro-conductive layer, Appl. Surf. Sci. 331 (2015) 309-314.

[9] D. Hong, Y. Guo, H. Wang, J. Zhou, H. Fang, Mechanism for improving the cycle performance of $LiNi_{0.5}Mn_{1.5}O_4$ by RuO_2 surface modification and increasing discharge cut-off potentials, J. Mater. Chem. A 3 (2015) 15457-15465.

[10] H.B. Kang, S.T. Myung, K. Amine, S. M. Lee, Y.K. Sun, Improved

electrochemical properties of BiOF-coated 5 V spinel $Li[Ni_{0.5}Mn_{1.5}]O_4$ for rechargeable lithium batteries, J. Power Sources 195 (2010) 2023-2028.

[11] H. Konishi, K. Suzuki, S. Taminato, K. Kim, Y. Zheng, S. Kim, J. Lim, M. Hirayama, J.Y. Son, Y. Cui, R. Kanno, Effect of surface Li_3PO_4 coating on $LiNi_{0.5}Mn_{1.5}O_4$ epitaxial thin film electrodes synthesized by pulsed laser deposition, J. Power Sources 269 (2014) 293-298.

[12] J. W. Kim, D. H. Kim, D. Y. Oh, H. Lee, J. H. Kim, J. H. Lee, Y. S. Jung, Surface chemistry of $LiNi_{0.5}Mn_{1.5}O_4$ particles coated by Al_2O_3 using atomic layer deposition for lithium-ion batteries, J. Power Sources 274 (2015) 1254-1262.

[13] J. Li, Y. Zhang, J. Li, L. Wang, X. He, J. Gao, AlF_3 coating of $LiNi_{0.5}Mn_{1.5}O_4$ for high-performance Li-ion batteries, Ionics 17 (2011) 671-675.

[14] D. H. Wang, D. W. Choi, J. Li, Z. G. Yang, Z. M. Nie, R. Kou, D. H. Hu, C. M. Wang, L. V. Saraf, J. G. Zhang, Self-assembled TiO_2-graphene hybrid nanostructures for enhanced Li-ion insertion, ACS Nano 3 (2009) 907-914.

[15] C.V. Rao, A. L. M. Reddy, Y. Ishikawa, P. M. Ajayan, $LiNi_{1/3}Co_{1/3}Mn_{1/3}O_2$-graphene composite as a promising cathode for lithium-ion batteries, Appl. Mater. Interfaces 3 (2011) 2966-2972.

[16] X. Zhou, F. Wang, Y. Zhu, Z. Liu, Graphene modified $LiFePO_4$ cathode materials for high power lithium ion batteries, J. Mater. Chem. 21 (2011) 3353-3358.

[17] B. Song, M. O. Lai, Z. Liu, H. Liu, L. Lu, Graphene-based surface modification on layered Li-rich cathode for high-performance Li-ion batteries, J. Mater. Chem. A 1 (2013) 9954-9965.

[18] S. J. R. Prabakar, Y.H. Hwang, B. Lee, K.S. Sohn, M. Pyo, Graphene-sandwiched $LiNi_{0.5}Mn_{1.5}O_4$ cathode composites for enhanced high voltage performance in Li ion batteries, J. Electrochem. Soc. 160 (2013) A832-A837.

[19] M. H. Pyun, Y. J. Park, Graphene/$LiMn_2O_4$ nanocomposites for enhanced lithium ion batteries with high rate capability, J. Alloys Compd. 643 (2015) s90-s94.

[20] S. Pei, H.-M. Cheng, The reduction of graphene oxide, Carbon 50 (2012) 3210-3228.

[21] J. G. Radich, P. V. Kamat, Origin of reduced graphene oxide enhancements in electrochemical energy storage, ACS Catal. 2 (2012) 807-816.

[22] M. Mo, C. Ye, K. Lai, Z. Huang, L. Zhu, G. Ma, H. Chen, K.S. Hui, Gelatin-assisted synthesis of $LiNi_{0.5}Mn_{1.5}O_4$ cathode material for 5 V lithium rechargeable batteries, Appl. Surf. Sci. 276 (2013) 635-640.

[23] D. Liu, J. Hamel-Paquet, J. Trottier, F. Barray, V. Gariépy, P. Hovington, A. Guerfi, A. Mauger, C.M. Julien, J.B. Goodenough, K. Zaghi, Synthesis of pure phase disordered $LiMn_{1.45}Cr_{0.1}Ni_{0.45}O_4$ by a post-annealing method, J. Power Sources 217 (2012) 400-406.

[24] K.C. Jiang, S. Xin, J. S. Lee, J. Kim, X.L. Xiao, Y.G. Guo, Improved kinetics of $LiNi_{1/3}Mn_{1/3}Co_{1/3}O_2$ cathode material through reduced graphene oxide networks, Phys. Chem. Chem. Phys. 14 (2012) 2934-2939.

[25] J. S. Park, K. C. Roh, J.W. Lee, K. Song, Y. Kim, Y. M. Kang, Structurally stabilized $LiNi_{0.5}Mn_{1.5}O_4$ with enhanced electrochemical properties through nitric acid treatment, J. Power Sources 230 (2013) 138-142.

[26] Y. Zhou，Q. Bao，Lal. Tang，Y. Zhong，K. P. Loh, Hydrothermal dehydration for the “green” reduction of exfoliated graphene oxide to graphene and demonstration of tunable optical limiting properties, Chem. Mater. 21 (2009) 2950-2956.

[27] N. P. W. Pieczonka, Z. Liu, P. Lu, K. L. Olson, J. Moote, B. R. Powell, J. H. Kim, Understanding transition-metal dissolution behavior in $LiNi_{0.5}Mn_{1.5}O_4$ high-voltage spinel for lithium ion batteries, J. Phys. Chem. C 117 (2013) 15947-15957.

[28] R. Qiao, Y. Wang, P. Olalde-Velasco, H. Li, Y.-S. Hu, W. Yang, Direct evidence of gradient Mn(II) evolution at charged states in $LiNi_{0.5}Mn_{1.5}O_4$ electrodes with capacity fading, J. Power Sources 273 (2015) 1120-1126.

[29] M. Mo, K.S. Hui, X. Hong, J. Guo, C. Ye, A. Li, N. Hu, Z. Huang, J. Jiang, J. Liang, H. Chen, Improved cycling and rate performance of Sm-doped $LiNi_{0.5}Mn_{1.5}O_4$ cathode materials for 5 V lithium ion batteries, Appl. Surf. Sci. 290 (2014) 412-418.

Captions for Figures

Fig. 1 XRD patterns of LNMO, rGO-LNMO and rGO

Fig. 2 Raman spectra for (a) rGO-LNMO, (b) GO and (c) rGO.

Fig. 3 (a，b) SEM micrographs of rGO-LNMO

Fig. 4 The EDX elemental mapping of rGO-LNMO under SEM

Fig. 5 (a) C 1s, (b) Mn 2p and Ni 2p peak fitting results of the XPS spectra of GO, LNMO and rGO-LNMO

Fig. 6 (a) Charge-discharge profiles at 0.1 C, (b) Cyclic voltammograms, (c) Cyclic performance cycled at 1 C, and (d) The rate performance of LNMO and the rGO-LNMO samples.

Fig. 7 EIS of spinel LNMO and rGO-LNMO

Figures

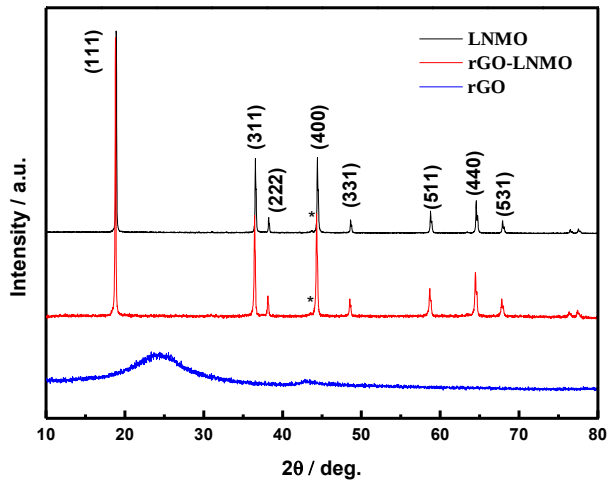

Figure 1

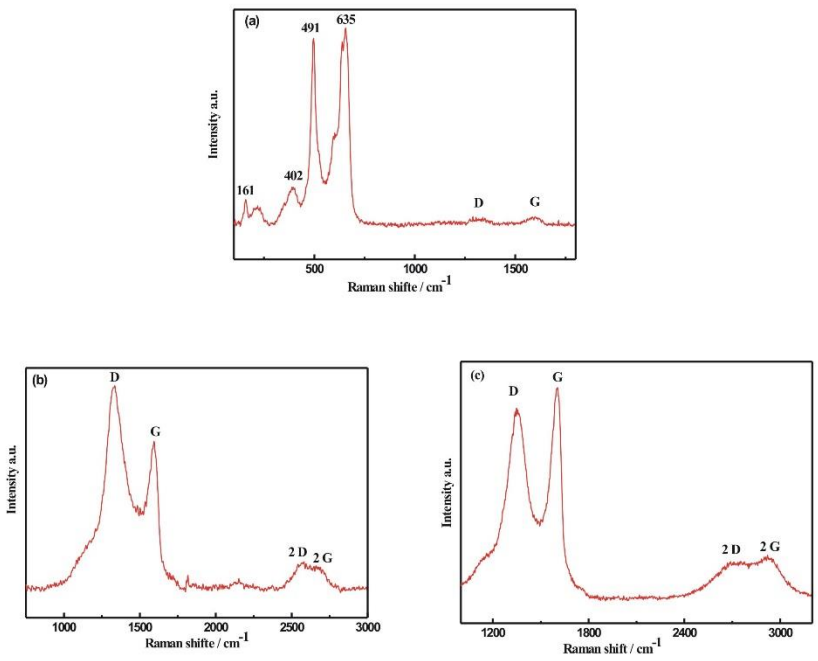

Figure 2

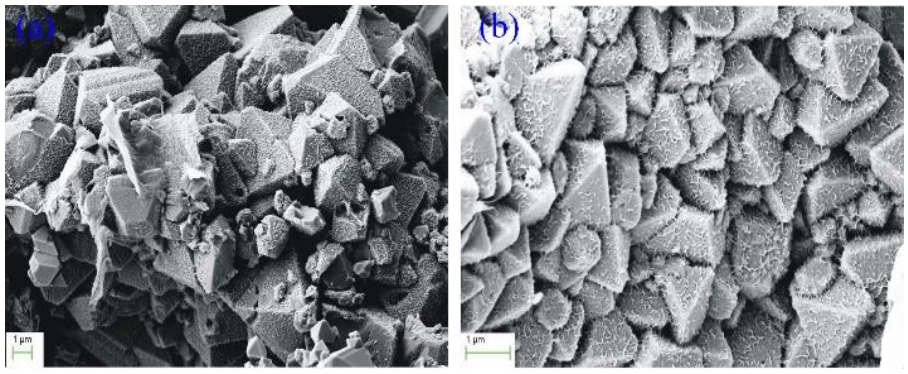

Figure 3

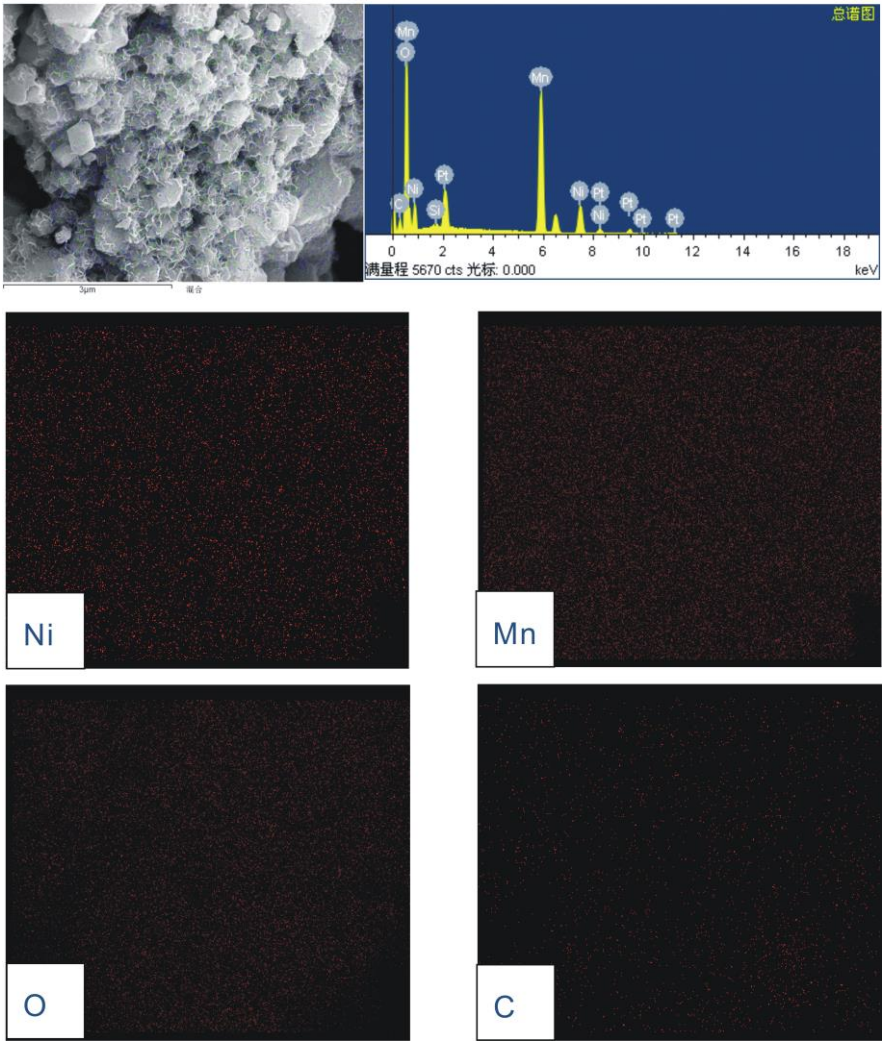
总谱图
Mn
O
Pt
Ni
C
Si
0 2 4 6 8 10 12 14 16 18
满量程 5670 cts 光标: 0.000
keV
Ni
Mn
O
C

Figure 4

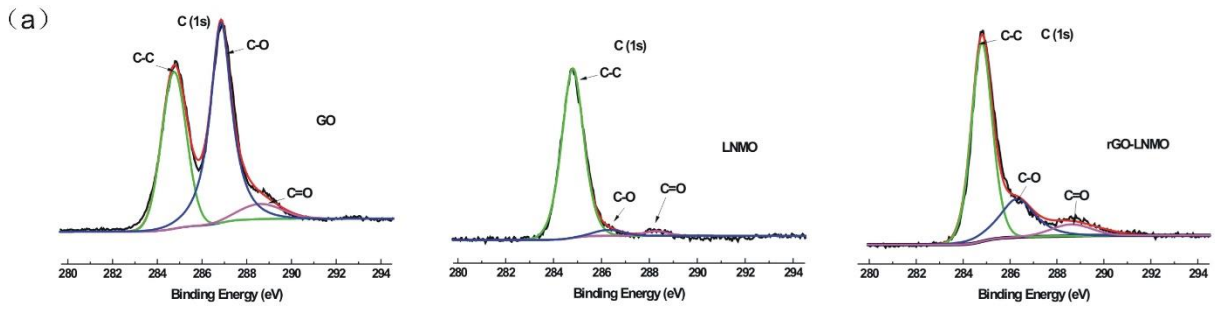
(a)
C (1s)
C-C
C-O
C=O
GO
LNMO
rGO-LNMO
280 282 284 286 288 290 292 294
Binding Energy (eV)

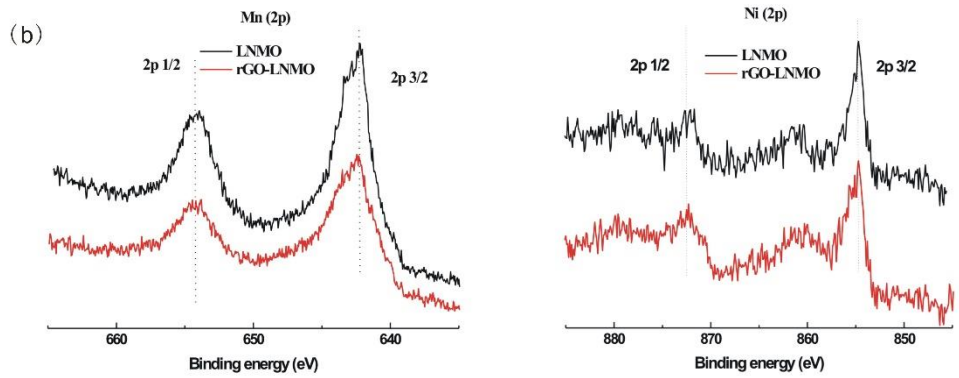

1

2

3 Figure 5

4

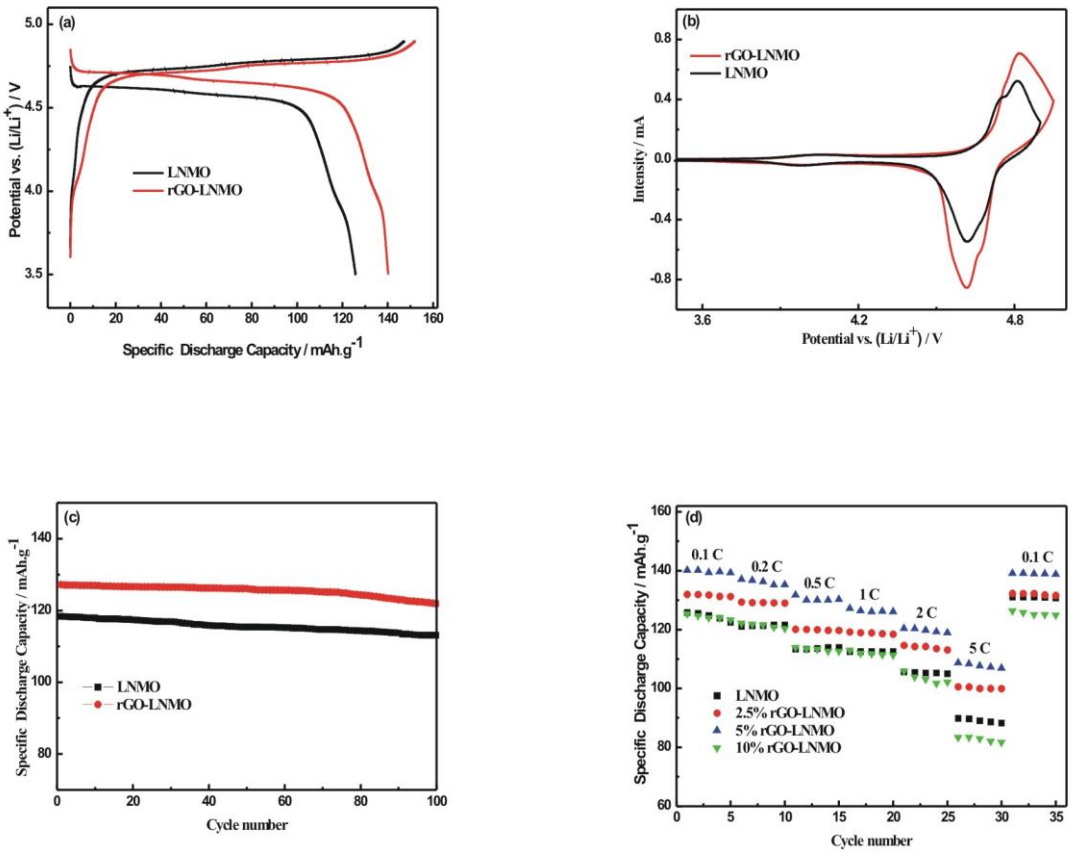

5

6

7 Figure 6

8

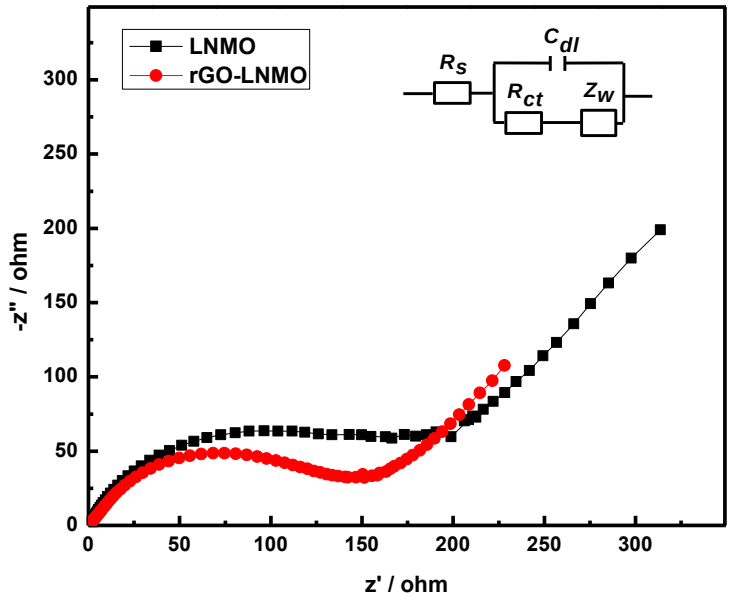

Figure 7

Supporting Information

Fig. S1 The nitrogen adsorption–desorption isotherm of (a) $LiNi_{0.5}Mn_{1.5}O_4$ and (b) rGO-LNMO

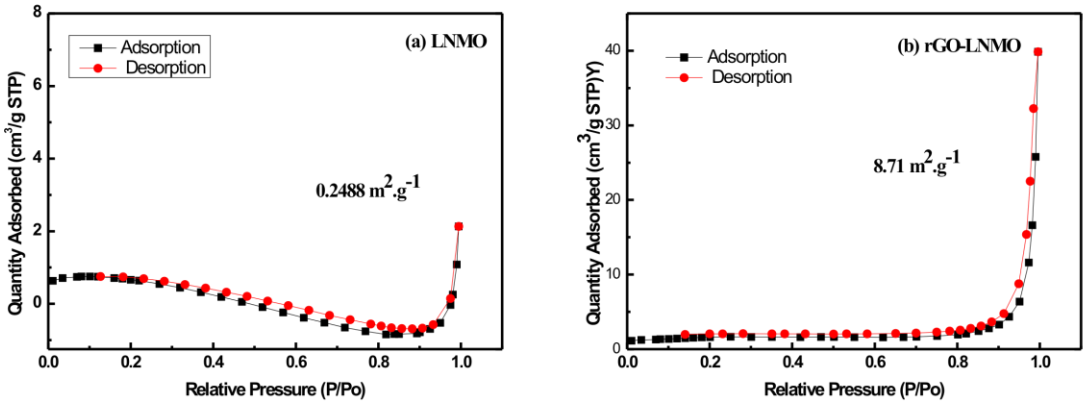

Figure S1